

Slow and velocity-tunable beams of metastable He₂ by multistage Zeeman decelerationMichael Motsch,^{*} Paul Jansen, Josef A. Agner, Hansjürg Schmutz, and Frédéric Merkt[†]*Laboratorium für Physikalische Chemie, ETH Zürich, CH-8093 Zürich, Switzerland*

(Received 28 January 2014; published 21 April 2014)

We report on the use of multistage Zeeman deceleration to generate beams of He₂ molecules in the metastable $a^3\Sigma_u^+$ state with velocities tunable down to 100 m/s. The metastable molecules are generated by striking a discharge in a supersonic expansion of pure helium gas from a pulsed valve held at cryogenic temperature. The velocity and internal-state distributions of the metastable He₂ molecules are measured for nozzle temperatures of 300, 77, and 10 K by high-resolution photoelectron and photoionization spectroscopy. The deceleration process does not exhibit any rotational state selectivity with rotational levels up to $N'' = 21$ being populated, but eliminates molecules in spin-rotational sublevels with $J'' = N''$ from the beam, where J'' and N'' are the total and the rotational angular momentum quantum number, respectively. The lack of rotational state selectivity is attributed to the fact that the Paschen-Back regime of the Zeeman effect in the rotational levels of He₂ is already reached at fields of only 0.1 T.

DOI: [10.1103/PhysRevA.89.043420](https://doi.org/10.1103/PhysRevA.89.043420)

PACS number(s): 37.10.-x, 37.20.+j

I. INTRODUCTION

In the past decade, several methods have become available to prepare molecules in the gas phase at low temperatures [1–4]. Going beyond thermalization with a cold environment, these methods allow for precise control of the external and internal degrees of freedom in molecular samples. Cold molecules with translational temperatures in the range from 100 mK to 1 K may then find applications in precision spectroscopy [5,6] and in the study of chemical reactivity at very low collision energies and very high energy resolution [7,8]. Alternatively, they may also represent the starting point for further cooling steps toward the ultracold regime below 1 mK [9–13]. The choice of the cooling method depends on the properties of the species of interest [2,14,15]. In the case of paramagnetic atoms and molecules that can be entrained in a supersonic beam, multistage Zeeman deceleration [16] and related techniques [17,18] are the methods of choice: The phase-space density of atoms and molecules in supersonic beams is high and is preserved by phase-stable operation of the decelerator [19,20], the method can be quantum-state selective [21], the final velocity of the particles can be controlled and tuned over a wide range [22–24], and the decelerated particles can be loaded into a magnetic trap [25,26] for observation of slow decay processes or spectroscopic measurements requiring long observation times.

We describe here the use of multistage Zeeman deceleration to generate slow and velocity-tunable beams of He₂ molecules in the metastable $a^3\Sigma_u^+$ state (referred to as He₂^{*} hereafter) in a setup tailored for future applications in precision spectroscopy. We also demonstrate the possibility to use the cold molecular samples to study the rovibrational energy-level structure of the $a^3\Sigma_u^+$ state of He₂ and the $X^+2\Sigma_u^+$ ground state of He₂⁺ by photoionization and photoelectron spectroscopic methods. Being three- and four-electron systems, respectively, He₂ and He₂⁺ represent attractive systems to test the accuracy of *ab initio* quantum-chemical methods. In the

two-electron systems H₂, HD, and D₂, the results of *ab initio* calculations of dissociation energies and rovibrational energy levels, which include adiabatic and nonadiabatic corrections to the Born-Oppenheimer approximation as well as quantum-electrodynamics corrections up to the leading (one-loop) contribution to the term proportional to α^4 , were found to be in agreement with experimental results within the combined uncertainties of the experimental and theoretical determinations [27–34]. Such calculations become increasingly challenging as the number of electrons increases and the magnitudes of the relativistic and quantum-electrodynamics corrections are not accurately known for He₂⁺. In a recent high-resolution spectroscopic study of the threshold ionization spectrum of He₂^{*}, the level spacings between the lowest four rotational levels of He₂⁺ could be determined at an accuracy of 100 MHz [35]. Comparison with the latest *ab initio* calculations neglecting quantum-electrodynamics corrections [36] did not reveal significant deviations from the experimental results at this level of accuracy, except perhaps for the highest rotational level observed experimentally. In the future, we would like to improve the accuracy of these measurements by using a slow beam of metastable He₂, which motivated us to develop a He₂^{*} source better suited to precision spectroscopic experiments.

As a starting point, a supersonic beam of He₂^{*} was produced with a pulsed source operated at cryogenic temperatures. The velocity of the molecules was subsequently reduced to ≈ 100 m/s by coupling the cryogenic beam source to a multistage Zeeman decelerator. From pulsed-field-ionization-zero-kinetic-energy (PFI-ZEKE) photoelectron spectra of the $X^+2\Sigma_u^+ \leftarrow a^3\Sigma_u^+$ transition, we have determined the internal-state distribution of the cold molecules in the beam and found rotational states up to $N'' = 21$ to be populated. Deceleration experiments with these molecules enabled the study of the rotational state selectivity of the deceleration process. The comparison with the deceleration of molecular oxygen (O₂) in the $X^3\Sigma_g^-$ state, for which full selectivity of the spin-rotational state $|\tilde{N} = 1, J = 2, M_J = 2\rangle$ was achieved [21], revealed striking differences that are attributed to the different nature of the Zeeman effect in these two molecular systems.

^{*}michael.motsch@phys.chem.ethz.ch[†]frederic.merkt@phys.chem.ethz.ch

II. EXPERIMENT

He_2^* is formed in a gas of pure helium under conditions where the density allows for three-body collisions on the relevant time scales and collision partners of sufficiently high energy are available to excite helium atoms to their metastable states. Such conditions typically prevail in plasmas, such as those generated by striking an electric discharge through helium gas [37,38]. The large ratio of magnetic moment to mass makes He_2^* particularly attractive for multistage Zeeman deceleration. Moreover, the predicted radiative lifetime of 18 s of He_2^* [37] is sufficiently long that no decay takes place on the millisecond time scale of the deceleration process. However, the high velocity (about 2000 m/s) of a supersonic expansion of pure He from a reservoir held at room temperature poses a problem. For the multistage Zeeman decelerator used in our experiments, the deceleration-solenoid geometry and the 8- μs switching times of the pulsed deceleration magnetic fields limit the maximal initial velocity of the particles to be decelerated to about 700 m/s [2,20]. The common approach to produce low-velocity supersonic beams consisting of seeding the species of interest in a heavy rare gas is not an option in the case of He^* and He_2^* because these metastable species carry sufficient internal energy to cause the Penning ionization of all other rare gases [39]. The operation of the pulsed-valve assembly, including discharge electrodes, at cryogenic temperatures is therefore the only viable option to reduce the initial velocity of the supersonic beam to below 700 m/s.

To produce slow and velocity-tunable beams of metastable helium molecules at low speed, we have combined a pulsed cryogenic supersonic beam source with a multistage Zeeman

decelerator in the experimental setup depicted schematically in Fig. 1(a). The setup consists of the pulsed-valve assembly with discharge electrodes, the actual multistage Zeeman decelerator, and a detection region where the metastable molecules are photoionized with UV laser radiation and the ions or electrons are extracted in the direction perpendicular to the beam propagation axis toward a microchannel-plate (MCP) detector. The Zeeman decelerator and the procedure used to achieve phase-stable deceleration were described in detail in Ref. [23]. Consequently, only the beam source is presented in detail in the following description of the experimental setup and procedure.

A. Cryogenic discharge source

The pulsed supersonic beam is created by expanding helium gas into vacuum from a reservoir held at high stagnation pressure (typically 2–6 bars) through the 250- μm -diameter ceramic orifice of a modified Even-Lavie valve [40]. To efficiently cool the valve, its entire housing, originally made of stainless steel, was replaced by copper components. The valve assembly was mounted onto the copper baseplate of a ≈ 0.7 l cylindrical container that can be filled with cryogenic liquids, either liquid nitrogen for operation at 77 K or liquid helium for operation down to 4 K. The temperature of the valve assembly was monitored with a silicon diode (Lakeshore DT-670) directly attached to it. Throughout this paper, we refer to the temperature measured with this sensor as the source temperature.

Starting with the valve assembly at room temperature, it takes about 2 h until the valve and discharge operate stably at about 10 K. Once the desired final temperature is reached, the nozzle-assembly temperature is actively stabilized with a resistive heater attached to the valve. With feedback from a closed-loop proportional-integral-derivative controller (Lakeshore 336), the source temperature fluctuates by less than 0.1 K and conditions remain stable for several hours.

The metastable helium molecules are generated by striking a discharge and forming a plasma in the expansion region. For this purpose, the expanding gas passes through a 10-mm-long, 1.6-mm-diameter channel defined by two cylindrical electrodes directly attached to the front plate of the valve and separated by an electrically insulating sapphire spacer (2 mm in length with an inner diameter of the cylindrical channel of 2 mm). The discharge is ignited by applying a typically 5- μs -long, -600 -V pulse to the front electrode as soon as the density of the helium beam in the channel is sufficiently high. In the discharge, the metastable ($1s$)($2s$) 1S_0 and 3S_1 states of atomic helium are populated and the metastable helium dimer molecules are formed. To facilitate ignition of the discharge during the short duration of the gas pulse (typically a few tens of microseconds), the discharge is seeded with electrons emitted from a hot tungsten filament [23,41] and attracted toward the channel by a 200-V bias on the front electrode. Without the filament, ignition of the discharge required much higher electric potentials, which unnecessarily heated the beam. The discharge and nozzle operation parameters (electric potentials, timing, and stagnation pressure) were optimized by monitoring the yield of He_2^* with the methods described in Sec. II C.

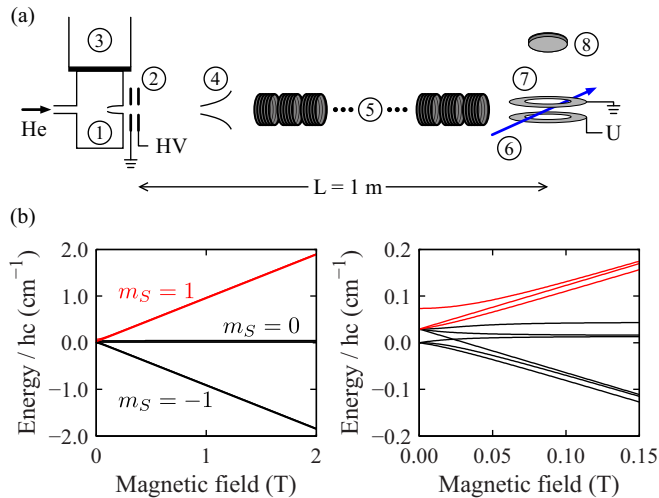


FIG. 1. (Color online) (a) Schematic representation of the experimental setup (not to scale): 1, pulsed-valve body and orifice; 2, discharge electrodes; 3, cryogenic-liquid container; 4, skimmer; 5, multistage Zeeman decelerator; 6, UV laser beam; 7, extraction electrodes; and 8, MCP. The supersonic beam propagation direction, the UV laser beam, and the ion extraction direction are mutually orthogonal. (b) Zeeman effect in the $N'' = 1$ rotational ground state of He_2 ($\alpha^3\Sigma_u^+$). The low-field-seeking states, for which the deceleration pulse sequence is optimized, are indicated in red. The low-field regime of the Zeeman effect is depicted in the right panel. HV = high-voltage supply for discharge. U = high-voltage supply for ion extraction.

We have also tested other discharge-electrode designs (e.g., high electric potential applied to a sharp tip in the expansion region [23,41] and cylindrical electrodes surrounding a glass capillary) and found the best yield of He_2^* with the channel described above. All discharge configurations produced beams of metastable helium atoms, but He_2^* was only observed in the configuration described above.

In the experiment, we observed a strong influence of the discharge-electrode temperature on the final velocity of the beam of metastable helium atoms and molecules. This observation may be explained by the discharge electrodes being part of the channel through which the gas expands, thus constituting a virtual gas reservoir for the expansion and beam-formation process. To cool this critical part of the setup to the lowest possible temperatures, the discharge assembly was mechanically connected and thermally linked to the copper front plate of the valve body. Moreover, the valve and discharge assembly were surrounded by a thermal shield cooled with liquid nitrogen, which served the purpose of minimizing the heat load of thermal radiation from the hot filament and from components of the vacuum chamber at room temperature.

For fast data acquisition in spectroscopic experiments, the source can be operated at the full repetition rate of 25 Hz of the Nd:YAG-pumped dye-laser system used to detect the metastable molecules. In this case, a 650-l/s (nominal pumping speed for He) turbo molecular pump sufficed to maintain the pressure in the source vacuum chamber in the 10^{-5} -mbar range. After the formation of He_2^* molecules, the supersonic beam passed through the 2-mm-diameter hole of a skimmer, which separates the source chamber from the multistage Zeeman decelerator or the photoelectron spectrometer used to characterize the beam properties and guarantees efficient differential pumping.

B. Multistage Zeeman decelerator

The multistage Zeeman decelerator used in the present work consists of an array of deceleration solenoids to which current pulses are applied and was described in Ref. [23]. The deceleration results from the force

$$\vec{f}_Z = -\nabla E_Z = \nabla(\vec{\mu}_{\text{mag}} \cdot \vec{B}) \quad (1)$$

that acts on a paramagnetic atom or molecule with magnetic moment $\vec{\mu}_{\text{mag}}$ and Zeeman energy shift E_Z in the presence of an inhomogeneous magnetic field \vec{B} . Particle-trajectory simulations indicated that 55 deceleration stages operated at a current of 300 A suffice to fully decelerate a beam of He_2^* with an initial velocity of about 500 m/s. The 55 solenoids (with a length of 7.2 mm, 64 windings in four layers, and a 7.0-mm inner diameter) used as deceleration stages were grouped in two 12-stage modules and one 31-stage module. These modules were separated by pumping towers, as depicted in Fig. 2 of Ref. [23].

The Zeeman effect in the lowest rotational level ($N'' = 1$) of the metastable $a^3\Sigma_u^+$ state of He_2 is depicted in Fig. 1(b), where the low-field-seeking magnetic sublevels ($m_S = 1$, drawn in red) suitable for deceleration experiments have a magnetic moment corresponding to two Bohr magnetons. Because the spin-rotation coupling constant of low vibrational levels of

the $a^3\Sigma_u^+$ state of He_2 is very small [42], the Zeeman effect in higher rotational levels follows the same pattern as in the $N'' = 1$ level (see also the discussion at the end of Sec. III C). To generate beams of He_2^* with velocities in the range 100–150 m/s, the decelerator was operated at a repetition rate of 8.3 Hz by applying 250-A current pulses to the deceleration solenoids, resulting in maximal magnetic fields on the decelerator axis of about 1.8 T and Zeeman shifts of about 1.6 cm^{-1} for the low-field-seeking magnetic sublevels. The pulse sequences were precalculated to reach the desired final velocities for molecules in these sublevels. Optimal conditions were obtained for phase angles between 35° and 45° , as in our previous deceleration experiments with deuterium atoms [20], metastable Ne [23], and O_2 [21].

C. State-selective detection of the metastable He_2 molecules

The electric discharge described in Sec. II A leads to the production of metastable He atoms in the $(1s)(2s) \ ^1S_0$ and $\ ^3S_1$ states and of metastable He_2 molecules in the $a^3\Sigma_u^+$ state. Because both atoms and molecules are entrained at the same velocity in the supersonic expansion, they cannot be distinguished on the basis of their times of flight to a detector placed along the propagation axis of the supersonic beam. To observe the atoms and the molecules separately, they were photoionized with UV laser radiation produced by second-harmonic generation of a Nd:YAG-pumped pulsed dye laser and the photoions were extracted through a field-free time-of-flight tube toward a microchannel-plate detector using an electric-field pulse in the range 1000–2000 V/cm. The UV wave number ($34\,467 \text{ cm}^{-1}$) was chosen to be above the ionization threshold of the metastable $a^3\Sigma_u^+$ state of He_2 , in a region free of autoionization resonances, and also above that of the metastable $(1s)(2s) \ ^1S_0$ state of He. Consequently, both He^+ and He_2^+ were observed in the ion time-of-flight (TOF) spectrum, as is illustrated in Fig. 2. The enhanced electronic noise visible in the time-of-flight spectrum between 1.0 and $1.25 \mu\text{s}$ corresponds to the time at which the extraction field was applied, i.e., $1 \mu\text{s}$ after the laser pulse.

To measure the photoionization spectra of He_2^* , the signal was integrated over a time window centered at the arrival time

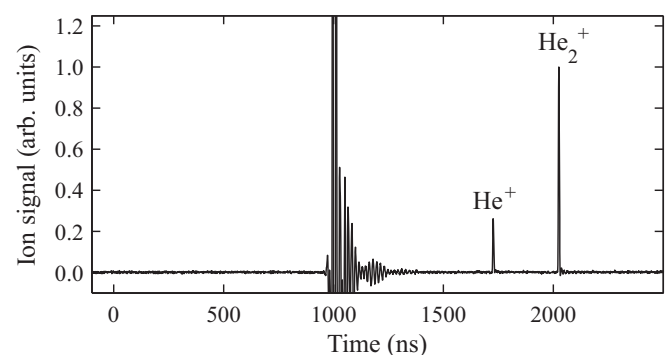


FIG. 2. Ion-TOF spectrum obtained following UV-laser photoionization at a wave number of $34\,467 \text{ cm}^{-1}$ and extracting the He^+ and He_2^+ ions with a pulsed extraction field applied $1 \mu\text{s}$ after the laser pulse. The electronic noise between 1.0– $1.25 \mu\text{s}$ is an artifact originating from the electric-field switch-on process.

of He_2^+ and recorded as a function of the excitation wave number, which was calibrated by recording the optogalvanic spectrum of Ne and the transmission through an étalon simultaneously with each spectrum. High-resolution photoelectron spectra of He_2^* were recorded using the technique of PFI-ZEKE photoelectron spectroscopy [43] following the same procedure as in our earlier study of the $\text{He}_2^+ X^+ 2\Sigma_u^+ \leftarrow \text{He}_2^* a^3\Sigma_u^+$ photoionizing transition [38]. The internal-state distribution of the metastable molecules was deduced from the rotational structure of the photoelectron spectra and the analysis of the Rydberg series observed in the photoionization spectra, as explained in Sec. III A.

The flight times of the metastable molecules from the point where they were generated in the discharge to the point where they were photoionized by the UV laser (called neutral-TOF spectra hereafter) were obtained by monitoring the resulting He_2^+ signal as a function of the delay time between the ignition of the discharge and the photoionization laser pulse. From the measured TOF distributions, the velocity distribution of the metastable molecules in the beam can be determined.

III. RESULTS AND DISCUSSION

A. Characterization of the supersonic beam

The He_2^* neutral-TOF spectra obtained for nozzle-assembly temperatures of 300, 77, and 10 K by varying the delay between the discharge ignition pulse and the firing of the ionization laser are compared in Fig. 3. Analyzing these neutral-TOF distributions following the procedure described in Refs. [2,23] enables one to extract, in each case, the average velocity of the molecular beam and the corresponding standard deviation, from which the translational temperature of the He_2^* sample can be estimated. From fits to the experimental time-of-flight profiles, the mean velocity and velocity spread of the beam are determined to be $\bar{v} = 1875, 975,$ and 530 m/s and $\sigma_v = 95, 65,$ and 60 m/s for source temperatures of 300, 77, and 10 K, respectively. When the valve body is stabilized to 10 K, the beam properties are sensitive to the discharge conditions, which results in day-to-day variations of the mean velocity by ± 10 m/s. The results of this analysis are summarized in Table I and indicate that the main effect of cooling the nozzle is a strong reduction of the average

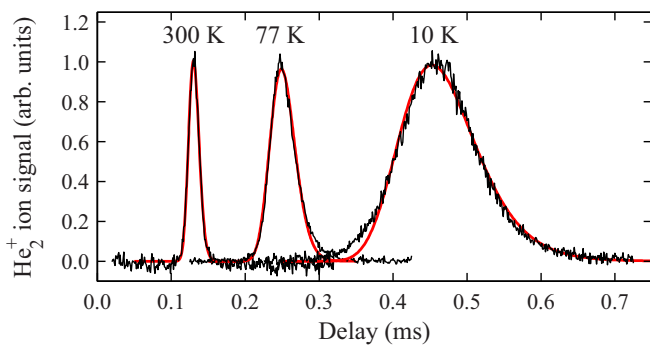


FIG. 3. (Color online) Plot of the He_2^* neutral-TOF spectra obtained for temperatures of the nozzle assembly of 300, 77, and 10 K. The red curves correspond to fits to the experimental data that led to the parameters summarized in Table I. See the text for details.

TABLE I. Parameters describing the velocity distribution of the beam of He_2^* obtained from an analysis of the neutral-TOF spectra shown in Fig. 3.

T_{source} (K)	\bar{v} (m/s)	σ_v (m/s)	T (K)
300	1875	95	4.4
77	975	65	1.9
10	530	60	1.8

velocity of the He_2^* molecules, the standard deviation being almost independent of the temperature of the nozzle assembly, particularly below 100 K.

The internal-state distribution of the molecular sample in the supersonic beam was determined from the rotational structure of the photoelectron spectrum of the origin band of the $\text{He}_2^+ X^+ 2\Sigma_u^+ \leftarrow \text{He}_2^* a^3\Sigma_u^+$ photoionizing transition. The photoelectron spectra obtained for nozzle-assembly temperatures of 10 and 300 K are displayed in Figs. 4(a) and 4(b), respectively. They were recorded using the technique of PFI-ZEKE photoelectron spectroscopy [43] by monitoring the delayed pulsed-field ionization of high Rydberg states (principal quantum number $n \geq 100$) located below the successive ionization thresholds of He_2^* as a function of the UV laser wave number. As explained in Ref. [38], removal of the $3s\sigma$ electron leads to a dominant Q -type rotational branch in the PFI-ZEKE photoelectron spectrum of He_2^* , corresponding to transitions between rotational levels of the neutral molecule and the ion having the same rotational quantum number, i.e., $\Delta N = N^+ - N'' = 0$ (N'' and N^+ are the rotational quantum numbers of He_2^* and He_2^+ , respectively). The positions of the Q -type transitions of the $v^+ = 0 \leftarrow v'' = 0$ band for N'' values between 1 and 21 are indicated along the upper assignment bar at the top of Fig. 4(a). Weak S -type lines (i.e., lines corresponding to $\Delta N = N^+ - N'' = 2$) are also observable in Fig. 4 and so are two strong and sharp autoionization resonances that strongly enhance the intensity of the $O(3)$ - and $O(5)$ -branch lines as a result of rotational channel interactions, as discussed in detail in Ref. [38]. The very weak lines corresponding to the lower assignment bar form the Q -type branch of the $v^+ = 1 \leftarrow v'' = 1$ band. The observation of these lines indicates that the $v'' = 1$ level of the $a^3\Sigma_u^+$ state of He_2 is weakly populated in the supersonic beam.

The higher signal-to-noise ratio obtained at a nozzle-assembly temperature of 10 K indicates that the density of He_2^* is almost an order of magnitude larger than when the nozzle assembly is operated at room temperature. Whereas the rotational-line-intensity distribution of the spectrum recorded following expansion from the 300-K nozzle is well described by a rotational temperature of about 150 K, the spectrum of the He_2^* sample obtained with the 10-K nozzle assembly is characterized by a bimodal rotational intensity distribution, with a cold component corresponding to a temperature of about 150 K for levels with $N'' \leq 7$ and a much hotter (nonthermal) component corresponding to rotational levels in the range $N'' = 9\text{--}21$ with a maximum at $N'' = 17$. The 10-K nozzle assembly thus leads to a rotationally warmer sample than the 300-K nozzle assembly. This somewhat

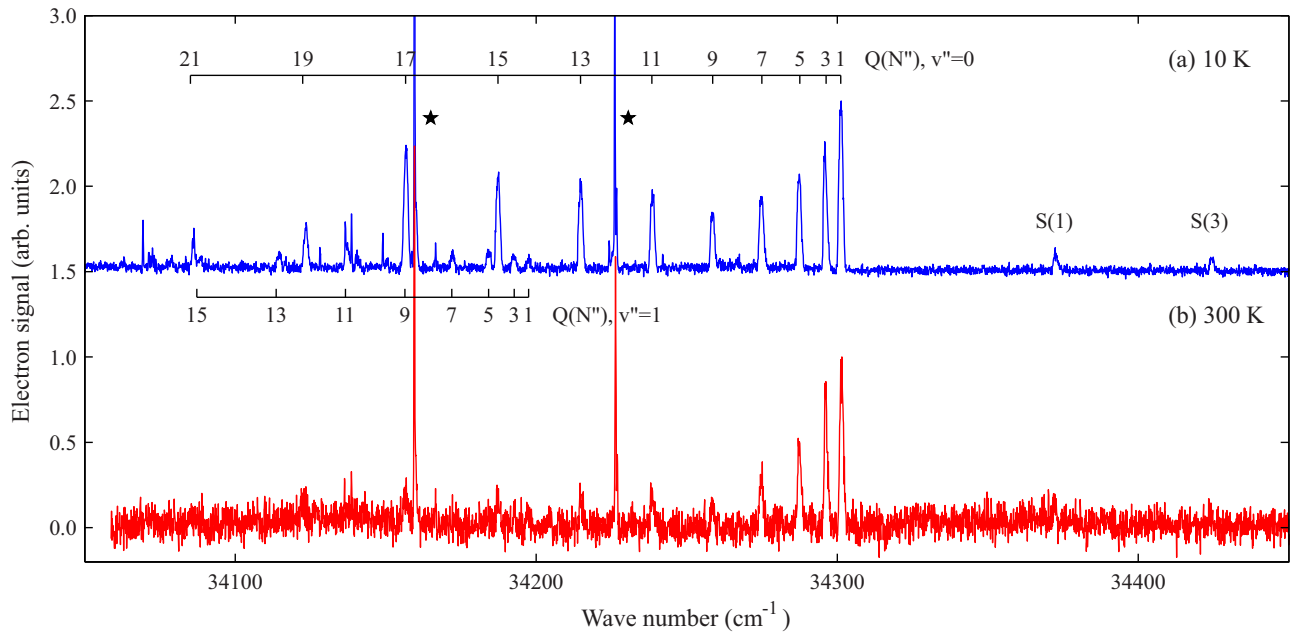


FIG. 4. (Color online) Plot of the PFI-ZEKE photoelectron spectra of the origin band of the $\text{He}_2^+ X^+ 2\Sigma_u^+ \leftarrow \text{He}_2^* a^3\Sigma_u^+$ photoionizing transition obtained for nozzle-assembly temperatures of (a) 10 K (blue trace) and (b) 300 K (red trace). The numbers along the upper and lower assignment bars represent the values of the rotational quantum number N'' of He_2^* of the dominant Q -type-branch (i.e., $\Delta N = N^+ - N'' = 0$) lines of the $v^+ = 0 \leftarrow v'' = 0$ and $v^+ = 1 \leftarrow v'' = 1$ bands, respectively. The weak lines designated as $S(1)$ and $S(3)$ are $\Delta N = N^+ - N'' = 2$ transitions originating from the rotational levels $N'' = 1$ and 3, respectively. The two strong, sharp lines marked by stars correspond to autoionization resonances, which strongly enhance the intensities of the $O(3)$ and $O(5)$ lines. The intensities in both spectra were normalized to the intensity of the $Q(1)$ transition. See the text for details.

counterintuitive observation may be explained by the large rotational constant [$B_0 = 7.101\,63(54)\text{ cm}^{-1}$ (see Ref. [38])] of He_2^* and the fact that only odd- N'' rotational levels of the $a^3\Sigma_u^+$ state are allowed by the generalized Pauli principle: The spacing between successive rotational levels rapidly becomes larger than the thermal collision energy when the nozzle assembly is held at low temperature and, consequently, cooling of the rotational degrees of freedom becomes very inefficient. The broad range of rotational states that are populated in the slow beam produced with the cold nozzle opens up the possibility to study levels with rotational energy exceeding 3000 cm^{-1} by high-resolution spectroscopy under the collision-free conditions of a supersonic beam.

B. Multistage Zeeman deceleration of He_2^*

When the nozzle assembly and the discharge electrodes are cooled down to about 10 K, the He_2^* molecules are entrained in a supersonic beam with a mean velocity of $\approx 500\text{ m/s}$, which is well below the maximal initial velocity tolerated by our Zeeman decelerator. As mentioned in Sec. II B, 55 deceleration stages grouped in three modules suffice to decelerate He_2^* to final velocities of 100 m/s.

Time-of-flight profiles of He_2^* detected at the exit of the Zeeman decelerator, i.e., at a distance of about 1 m from the nozzle orifice, are displayed in Fig. 5. These profiles were obtained by the procedure (UV-laser photoionization mass spectrometry) used to characterize the beam source and discussed in Sec. III A. To prevent the artificial enhancement of the photoionization signal of molecules in specific rotational levels of the $a^3\Sigma_u^+$ state, the UV-laser wave number was

kept fixed at $34\,467\text{ cm}^{-1}$, in a structureless region of the photoionization spectrum. In Fig. 5, the black trace, with

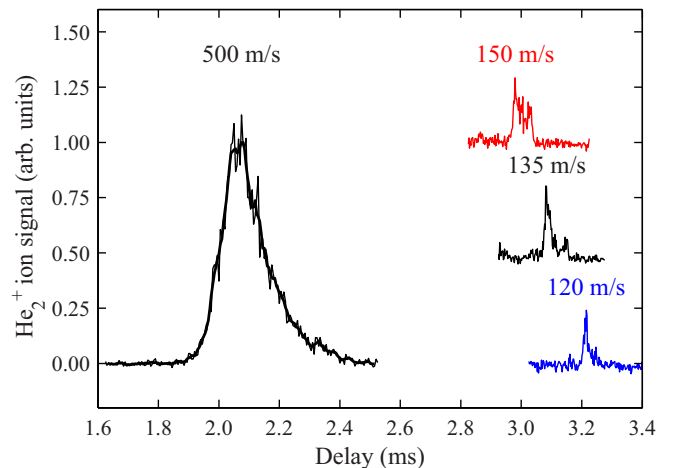


FIG. 5. (Color online) Time-of-flight profiles of He_2^* detected 60 mm beyond the last stage of the decelerator. The photoionization laser was set to $34\,467\text{ cm}^{-1}$, i.e., above all relevant ionization thresholds, to avoid the artificial enhancement of the photoionization signal of molecules in specific rotational levels of the $a^3\Sigma_u^+$ state. The black trace with a broad TOF distribution centered at 2.05 ms corresponds to the undecelerated beam. The three distributions presented at times of flight between 2.9 and 3.3 ms were obtained using deceleration pulse sequences designed to decelerate molecules with initial velocities of 505, 500, and 495 m/s, respectively, at a phase angle of 35° .

a broad peak of He_2^* molecules centered at a delay of 2.05 ms, represents the neutral TOF distribution recorded without switching any of the deceleration solenoids and corresponds to He_2^* molecules propagating at the original beam velocity of ≈ 500 m/s through the entire decelerator. When running the decelerator with current pulses of 250 A and a phase angle of 35° , the TOF profiles observed in the region between 2.9 and 3.3 ms were obtained. The profiles with maxima at 2.95 ms (red trace), 3.1 ms (black trace), and 3.25 ms (blue trace) were obtained under identical conditions except that the pulse sequences used for deceleration were precalculated to decelerate metastable molecules with initial velocities of 505, 500, and 495 m/s, respectively. Analysis of the time-of-flight profiles with the methods described in Ref. [23] indicates that the final velocities are 150, 135, and 120 m/s, respectively, in agreement with the values predicted by numerical particle-trajectory simulations. The structure of the peaks corresponding to the decelerated molecules is a consequence of the evolution of the phase-space distribution in the decelerator [20].

The neutral-TOF distributions presented in Fig. 5 demonstrate the possibility to tune the final velocity of the decelerated beam in the range between 100 and 150 m/s. Although the present setup allows for the deceleration to lower final velocities in a straightforward way, either by operating the decelerator at a larger phase angle or by applying larger deceleration magnetic fields, the detection of these slow molecules becomes increasingly difficult. In particular, the rather large distance of 60 mm between the last solenoid of the decelerator and the detection volume inevitably reduces the particle density by transverse defocusing and longitudinal dispersion effects, which play a larger role at lower final velocities [20]. For the efficient generation of beams with velocities below 100 m/s, deceleration pulse sequences with

optimized phase angles, such as those already used for trap-loading schemes [26], might be useful to focus and bunch the molecules into the detection region.

C. Spectroscopy and rotational-state distribution of the decelerated He_2^* beam

The maximum intensity of the peak in Fig. 5 corresponding to the decelerated He_2^* molecules is only a factor of 3 weaker than the maximum intensity of the undecelerated beam. Consequently, the internal-state distribution of the decelerated sample can be characterized by spectroscopic methods with almost the same sensitivity as achieved for the undecelerated beam (see Sec. III A). Unfortunately, it was not possible to record PFI-ZEKE photoelectron spectra in the region beyond the last coil of the decelerator. Indeed, the detection of the photoelectrons following extraction in the direction parallel to the beam propagation axis was hindered by the background signal originating from metastable atoms and molecules and electrons generated by the discharge. The stray magnetic fields along the decelerator axis further prevented the detection of electrons extracted in the direction perpendicular to the beam propagation axis. The internal-state distribution of the decelerated sample therefore had to be determined from the photoionization spectrum of He_2^* , which is dominated by contributions from autoionization resonances in the vicinity of the ionization thresholds (see Fig. 9 of Ref. [38]).

The photoionization spectra recorded in the region 34 125–34 185 cm^{-1} for decelerated and undecelerated He_2^* beams are compared in Fig. 6. These spectra are dominated by $N'' \rightarrow np(N^+ = N'')_{(N=N^+, N^+ \pm 1)}$ Rydberg series [35,38]. Whereas the $npN^+_{(N=N^+)}$ series, for which the character of the Rydberg electron is π_u^- , are regular and well described by Rydberg's formula, the $npN^+_{(N=N^+-1)}$ and $npN^+_{(N=N^++1)}$ series are of

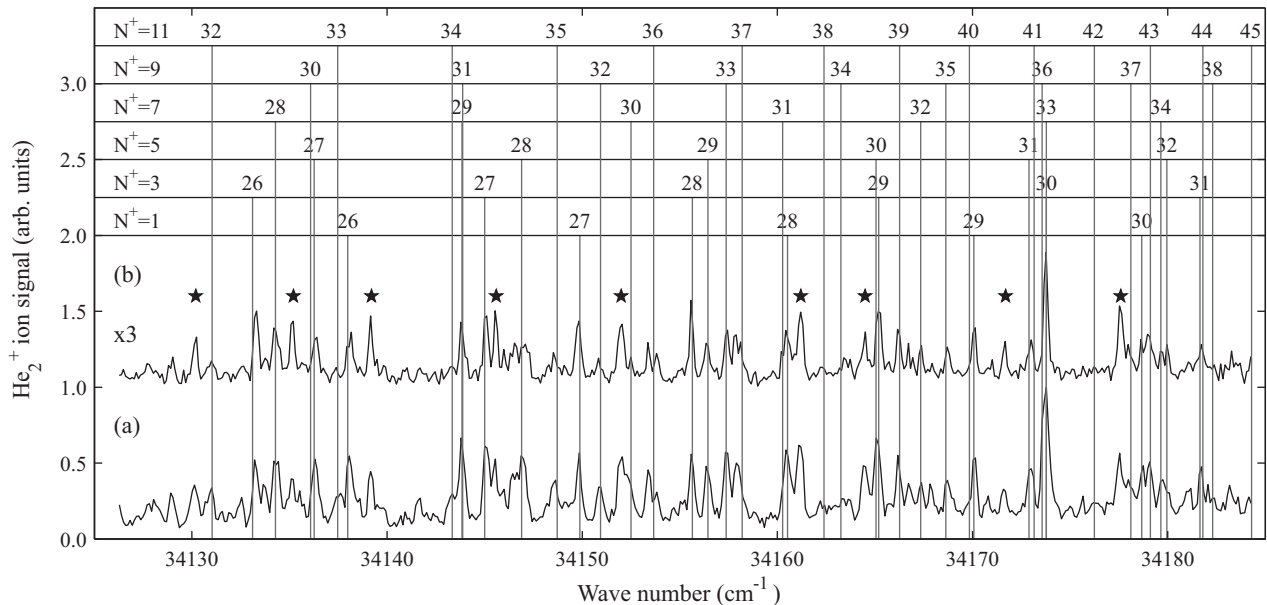


FIG. 6. Photoionization spectra of He_2 in the vicinity of the ionization threshold from the $a^3\Sigma_u^+$ state recorded for (a) an undecelerated beam and (b) a beam decelerated to a final velocity of 135 m/s. The assignment bars indicate the positions of the $N'' \rightarrow np(N^+ = N'')_{(N=N^+)}$ Rydberg states for $N^+ = 1-9$. The lines marked by stars belong to $N = N^+ \pm 1$ Rydberg series that are perturbed by rotational channel interactions. The intensity of trace (b) was multiplied by a factor of 3 and vertically offset for clarity.

mixed σ_u^+ and π_u^+ character and are strongly perturbed by rotational channel interactions with the $np(N^+ - 2)_{(N=N^+-1)}$ and $np(N^+ + 2)_{(N=N^++1)}$ series, respectively. For clarity, the assignments are only given for the regular series in Fig. 6 and the lines belonging to the perturbed series, which have also been assigned using the multichannel-quantum-defect-theory models described in Refs. [38,44], are marked by stars.

The unambiguous assignment of transitions originating from rotational levels of metastable He_2^* with N'' values between 1 and 9 demonstrates that many rotational levels are populated in the decelerated sample. Moreover, the almost identical appearance of the spectra of the decelerated and undecelerated samples presented in Fig. 6 implies that the multistage Zeeman deceleration process is not rotationally state selective in He_2^* . This observation stands in stark contrast to what is observed in the multistage Zeeman deceleration of O_2 , for which the decelerated sample was found to consist exclusively of molecules in the $M_J = 2$ magnetic sublevel of the $J = 2$ fine-structure component of the $N = 1$ rotational ground state [21]. The reason for the very different behaviors observed in O_2 and He_2^* lies in the different nature of the

Zeeman effect in these two molecules, which itself results from the fact that He_2^* has a much larger rotational constant than O_2 [$B_0 = 7.101\,63(54)\text{ cm}^{-1}$ [38] vs $1.437\,676\,38(55)\text{ cm}^{-1}$ [45,46]] and spin-rotational splittings more than two orders of magnitude smaller than O_2 [42].

The Zeeman effect in the ground vibrational level of O_2 $X^3\Sigma_g^-$ and He_2 $a^3\Sigma_u^+$ are compared in Fig. 7. In O_2 , the Paschen-Back regime is not reached at the magnetic fields up to 2 T used in our experiments because of the large fine-structure splitting of the rotational levels. Moreover, interactions between magnetic sublevels of the same M_J values but belonging to different rotational levels cause strong nonlinearities and avoided crossings already below 5 T. In He_2^* , the Paschen-Back regime is already reached at fields of less than 0.1 T and the large rotational spacings prevent any avoided crossings even at fields in excess of 15 T. Consequently, the low-field-seeking magnetic sublevels of the different rotational levels of He_2^* are subject to almost identical Zeeman shifts at the fields used in our deceleration experiments, which makes the deceleration process completely insensitive to the degree of rotational excitation.

Consideration of the Zeeman effect in the rotational levels of the $a^3\Sigma_u^+$ of He_2 , however, reveals that none of the magnetic sublevels of the spin-rotational levels with $J'' = N''$ are low-field seeking [see Fig. 7(d)]. Multistage Zeeman deceleration of He_2^* therefore acts as a filter that selects the two spin-rotational components with $J'' = N'' \pm 1$ and rejects the third.

IV. CONCLUSION

In this article, the design and operational characteristics of a source of slow, velocity-tunable beams of metastable He_2^* molecules (He_2^*) have been presented. The molecules are formed in a discharge, entrained in a supersonic expansion of He, and decelerated to low velocity in a multistage Zeeman decelerator. At the end of the decelerator, the density of He_2^* is sufficiently high for measurements of the Rydberg spectrum of He_2 by photoionization spectroscopy.

He_2 in its metastable $a^3\Sigma_u^+$ state has almost 20 eV of internal energy, which is enough to ionize any atom or molecule except He. Consequently, it is not possible to form a supersonic beam of He_2^* seeded in any carrier gas other than atomic helium. A supersonic beam of pure He expanding from a room-temperature reservoir has a mean velocity beyond the range of velocities for which deceleration is possible with our multistage Zeeman decelerator [23]. To overcome this limitation, we have developed a source that can be cooled to 10 K and at the exit of which He_2^* is generated in a discharge. He_2^* is then entrained by the He carrier gas in a supersonic beam having a mean velocity of about 500 m/s. Phase-stable deceleration to velocities as low as 100 m/s could be achieved using a Zeeman decelerator consisting of 55 stages. The velocity distribution of the decelerated molecules was measured by time-of-flight spectrometric methods and their internal-state distribution was determined from the analysis of well-resolved Rydberg series converging on the rovibrational levels of the $X^+2\Sigma_u^+$ ground electronic state of He_2^+ . The low translational temperature of the decelerated sample (less than 100 mK) and the broad range of populated rotational levels (N'' ranging from 1 to 21) make this source ideally

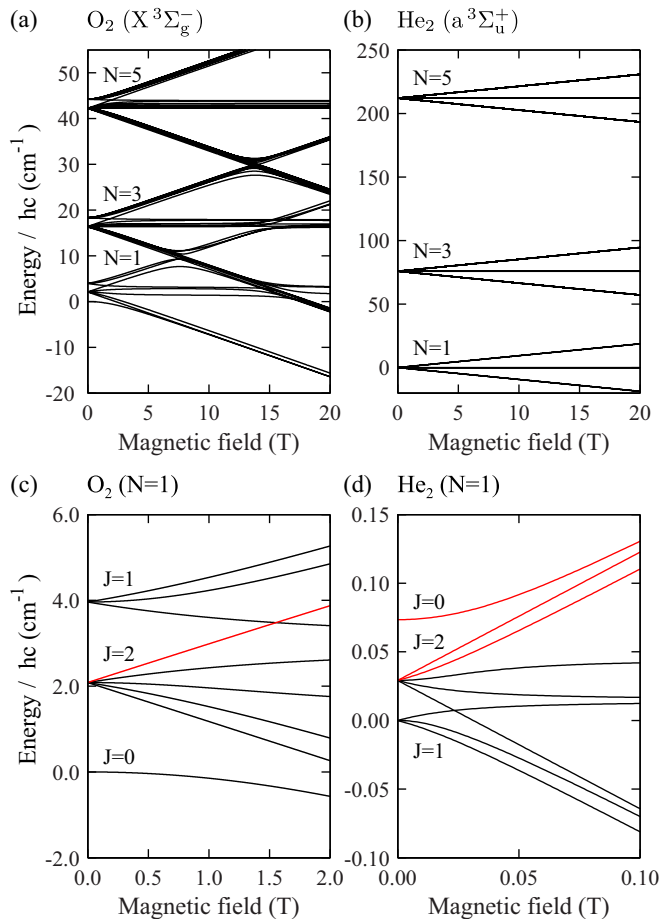


FIG. 7. (Color online) Comparison of the Zeeman effect in (a) and (c) the $X^3\Sigma_g^-$ ground state of O_2 and (b) and (d) the $a^3\Sigma_u^+$ state of He_2 (right column). (a) and (b) Zeeman energy of the rotational states $N'' = 1-5$ in the magnetic-field range between 0 and 20 T. (c) and (d) Zeeman energy in the magnetic-field range where the Zeeman shifts are comparable to the spin-rotation splittings. Note the different scales used in these panels.

suiting to measurements of the Rydberg spectrum of He₂, of the ionization energy of He₂^{*}, and of the rovibrational structure of He₂⁺ by high-resolution photoionization and photoelectron spectroscopic methods.

Unexpectedly, the population of metastable molecules in the supersonic expansion was found to be distributed over many more rotational levels when the valve was cooled down to low temperature than when it was operated at room temperature. We interpret this observation as arising from the fact that the rotational spacings in He₂^{*} are much larger than the thermal collision energy when the nozzle assembly is held at low temperature, which effectively hinders rotational cooling. The broad range of rotational levels in the supersonic expansion enabled us to study how the Zeeman deceleration process affects the rotational-state distribution. In contrast to O₂, for which multistage Zeeman deceleration led to the formation of slow beams of molecules in a single magnetic sublevel of a single spin-rotational level of the

ground electronic state [21], we did not observe any rotational state selectivity in the multistage Zeeman deceleration of He₂^{*}. We attribute this difference to the very different nature of the Zeeman effect in these two molecules (see Fig. 7). The deceleration process in He₂^{*}, however, rejects in each rotational level the spin-rotational component with $J'' = N''$. This property will represent an advantage in studies of the very congested Rydberg spectrum of He₂.

ACKNOWLEDGMENTS

We thank Richard Maceiczky and Patrick Seewald for their support in the early phase of this work. This work was supported by the Swiss National Science Foundation (Project No. 200020-149216) and the European Research Council advanced grant program (Project No. 228286). M.M. thanks ETH Zürich for support through an ETH fellowship.

-
- [1] M. T. Bell and T. P. Softley, *Mol. Phys.* **107**, 99 (2009).
- [2] S. D. Hogan, M. Motsch, and F. Merkt, *Phys. Chem. Chem. Phys.* **13**, 18705 (2011).
- [3] S. Y. T. van de Meerakker, H. L. Bethlem, N. Vanhaecke, and G. Meijer, *Chem. Rev.* **112**, 4828 (2012).
- [4] E. Narevicius and M. G. Raizen, *Chem. Rev.* **112**, 4879 (2012).
- [5] J. van Veldhoven, R. T. Jongma, B. Sartakov, W. A. Bongers, and G. Meijer, *Phys. Rev. A* **66**, 032501 (2002).
- [6] J. J. Hudson, D. M. Kara, I. J. Smallman, B. E. Sauer, M. R. Tarbutt, and E. A. Hinds, *Nature (London)* **473**, 493 (2011).
- [7] J. J. Gilijamse, S. Hoekstra, S. Y. T. van de Meerakker, G. C. Groenenboom, and G. Meijer, *Science* **313**, 1617 (2006).
- [8] M. Kirste, X. Wang, H. C. Schewe, G. Meijer, K. Liu, A. van der Avoird, L. M. C. Janssen, K. B. Gubbels, G. C. Groenenboom, and S. Y. T. van de Meerakker, *Science* **338**, 1060 (2012).
- [9] E. S. Shuman, J. F. Barry, D. R. Glenn, and D. DeMille, *Phys. Rev. Lett.* **103**, 223001 (2009).
- [10] E. S. Shuman, J. F. Barry, and D. DeMille, *Nature (London)* **467**, 820 (2010).
- [11] M. Zeppenfeld, B. G. U. Englert, R. Glöckner, A. Prehn, M. Mielenz, C. Sommer, L. D. van Buuren, M. Motsch, and G. Rempe, *Nature (London)* **491**, 570 (2012).
- [12] J. F. Barry, E. S. Shuman, E. B. Norrgard, and D. DeMille, *Phys. Rev. Lett.* **108**, 103002 (2012).
- [13] V. Zhelyazkova, A. Cournol, T. E. Wall, A. Matsushima, J. J. Hudson, E. A. Hinds, M. R. Tarbutt, and B. E. Sauer, [arXiv:1308.0421](https://arxiv.org/abs/1308.0421).
- [14] S. Y. T. van de Meerakker, H. L. Bethlem, and G. Meijer, *Nat. Phys.* **4**, 595 (2008).
- [15] M. Leshchko, R. V. Krems, J. M. Doyle, and S. Kais, *Mol. Phys.* **111**, 1648 (2013).
- [16] N. Vanhaecke, U. Meier, M. Andrist, B. H. Meier, and F. Merkt, *Phys. Rev. A* **75**, 031402(R) (2007).
- [17] A. Trimeche, M. Bera, J. Cromières, J. Robert, and N. Vanhaecke, *Eur. Phys. J. D* **65**, 263 (2011).
- [18] E. Lavert-Ofir, L. David, A. B. Henson, S. Gersten, J. Narevicius, and E. Narevicius, *Phys. Chem. Chem. Phys.* **13**, 18948 (2011).
- [19] H. L. Bethlem, F. M. H. Cromptoets, R. T. Jongma, S. Y. T. van de Meerakker, and G. Meijer, *Phys. Rev. A* **65**, 053416 (2002).
- [20] A. W. Wiederkehr, S. D. Hogan, and F. Merkt, *Phys. Rev. A* **82**, 043428 (2010).
- [21] A. W. Wiederkehr, H. Schmutz, M. Motsch, and F. Merkt, *Mol. Phys.* **110**, 1807 (2012).
- [22] E. Narevicius, A. Libson, C. G. Parthey, I. Chavez, J. Narevicius, U. Even, and M. G. Raizen, *Phys. Rev. Lett.* **100**, 093003 (2008).
- [23] A. W. Wiederkehr, M. Motsch, S. D. Hogan, M. Andrist, H. Schmutz, B. Lambillotte, J. A. Agner, and F. Merkt, *J. Chem. Phys.* **135**, 214202 (2011).
- [24] T. Momose, Y. Liu, S. Zhou, P. Djuricanin, and D. Carty, *Phys. Chem. Chem. Phys.* **15**, 1772 (2013).
- [25] S. D. Hogan, A. W. Wiederkehr, H. Schmutz, and F. Merkt, *Phys. Rev. Lett.* **101**, 143001 (2008).
- [26] A. W. Wiederkehr, S. D. Hogan, B. Lambillotte, M. Andrist, H. Schmutz, J. Agner, Y. Salathé, and F. Merkt, *Phys. Rev. A* **81**, 021402(R) (2010).
- [27] J. Liu, E. J. Salumbides, U. Hollenstein, J. C. J. Koelemeij, K. S. E. Eikema, W. Ubachs, and F. Merkt, *J. Chem. Phys.* **130**, 174306 (2009).
- [28] J. Liu, D. Sprecher, Ch. Jungen, W. Ubachs, and F. Merkt, *J. Chem. Phys.* **132**, 154301 (2010).
- [29] D. Sprecher, J. Liu, Ch. Jungen, W. Ubachs, and F. Merkt, *J. Chem. Phys.* **133**, 111102 (2010).
- [30] K. Pachucki and J. Komasa, *J. Chem. Phys.* **130**, 164113 (2009).
- [31] K. Piszczatowski, G. Łach, M. Przybytek, J. Komasa, K. Pachucki, and B. Jeziorski, *J. Chem. Theory Comput.* **5**, 3039 (2009).
- [32] G. D. Dickenson, E. J. Salumbides, M. Niu, C. Jungen, S. C. Ross, and W. Ubachs, *Phys. Rev. A* **86**, 032502 (2012).
- [33] D. Sprecher, Ch. Jungen, W. Ubachs, and F. Merkt, *Faraday Discuss.* **150**, 51 (2011).
- [34] G. D. Dickenson, M. L. Niu, E. J. Salumbides, J. Komasa, K. S. E. Eikema, K. Pachucki, and W. Ubachs, *Phys. Rev. Lett.* **110**, 193601 (2013).
- [35] D. Sprecher, J. Liu, T. Krähenmann, M. Schäfer, and F. Merkt, *J. Chem. Phys.* **140**, 064304 (2014).

- [36] W.-C. Tung, M. Pavanello, and L. Adamowicz, *J. Chem. Phys.* **136**, 104309 (2012).
- [37] C. F. Chabalowski, J. O. Jensen, D. R. Yarkony, and B. H. Lengsfeld, III, *J. Chem. Phys.* **90**, 2504 (1989).
- [38] M. Raunhardt, M. Schäfer, N. Vanhaecke, and F. Merkt, *J. Chem. Phys.* **128**, 164310 (2008).
- [39] P. E. Siska, *Rev. Mod. Phys.* **65**, 337 (1993).
- [40] U. Even, J. Jortner, D. Noy, N. Lavie, and C. Cossart-Magos, *J. Chem. Phys.* **112**, 8068 (2000).
- [41] T. Halfmann, J. Koensgen, and K. Bergmann, *Meas. Sci. Technol.* **11**, 1510 (2000).
- [42] C. Focsa, P. Bernath, and R. Colin, *J. Mol. Spectrosc.* **191**, 209 (1998).
- [43] G. Reiser, W. Habenicht, K. Müller-Dethlefs, and E. W. Schlag, *Chem. Phys. Lett.* **152**, 119 (1988).
- [44] D. Sprecher, Ch. Jungen, and F. Merkt, *J. Phys. Chem. A* **117**, 9462 (2013).
- [45] K. P. Huber and G. Herzberg, *Molecular Spectra and Molecular Structure, IV. Constants of Diatomic Molecules* (Van Nostrand Reinhold, New York, 1979).
- [46] L. Tomuta, M. Mizushima, C. J. Howard, and K. M. Evenson, *Phys. Rev. A* **12**, 974 (1975).